

Experimental investigation of basalt and peridotite oxybarometers: Implications for spinel thermodynamic models and Fe³⁺ compatibility during generation of upper mantle melts

FRED A. DAVIS^{1,2,*} AND ELIZABETH COTTRELL¹

¹National Museum of Natural History, Smithsonian Institution, Washington, D.C. 20560, U.S.A.

²Department of Earth and Environmental Sciences, University of Minnesota Duluth, Duluth, Minnesota 55812, U.S.A.

ABSTRACT

Peridotites dredged from mid-ocean ridges and glassy mid-ocean ridge basalts (MORB) transmit information about the oxygen fugacity (f_{O_2}) of Earth's convecting upper mantle to the surface. Equilibrium assemblages of olivine+orthopyroxene+spinel in abyssal peridotites and Fe³⁺/ΣFe ratios in MORB glasses measured by X-ray absorption near-edge structure (XANES) provide independent estimates of MORB source region f_{O_2} , with the former recording f_{O_2} approximately 0.8 log units lower than the latter relative to the quartz-fayalite-magnetite (QFM) buffer. To test cross-compatibility of these oxybarometers and examine the compositional effects of changing f_{O_2} on a peridotite plus melt system over a range of Earth-relevant f_{O_2} , we performed a series of experiments at 0.1 MPa and f_{O_2} controlled by CO-CO₂ gas mixes between QFM-1.87 and QFM+2.23 in a system containing basaltic andesite melt saturated in olivine, orthopyroxene, and spinel.

Oxygen fugacities recorded by each method are in agreement with each other and with the f_{O_2} measured in the furnace. Measurements of f_{O_2} from the two oxybarometers agree to within 1σ in all experiments. These results demonstrate that the two methods are directly comparable and differences between f_{O_2} measured in abyssal peridotites and MORB result from geographic sampling bias, petrological processes that change f_{O_2} in these samples after separation of melts and residues, or abyssal peridotites may not be residues of MORB melting.

As f_{O_2} increases, spinel Fe³⁺ concentrations increase only at the expense of Cr from QFM-1.87 to QFM-0.11. Above QFM, Al is also diluted in spinel as the cation proportion of Fe³⁺ increases. None of the three spinel models tested, MELTS (Ghiorso and Sack 1995), SPINMELT (Ariskin and Nikolaev 1996), and MELT_CHROMITE (Poustovetov and Roeder 2001), describe these compositional effects, and we demonstrate that MELTS predicts residues that are too oxidized by >1 log unit to have equilibrated with the coexisting liquid phase. Spinel generated in this study can be used to improve future thermodynamic models needed to predict compositional changes in spinels caused by partial melting of peridotites in the mantle or by metamorphic reactions as peridotites cool in the lithosphere.

In our experimental series, where the ratio of Fe₂O₃/FeO in the melt varies while other melt compositional parameters remain nearly constant, experimental melt fraction remains constant, and Fe³⁺ becomes increasingly compatible in spinel as f_{O_2} increases. Instead of promoting melting, increasing the bulk Fe³⁺/ΣFe ratio in peridotite drives reactions analogous to the fayalite-ferrosilite-magnetite reaction. This may partly explain the absence of correlation between Na₂O and Fe₂O₃ in fractionation-corrected MORB.

Keywords: Oxygen fugacity, XANES, spinel peridotite oxybarometry, electron microprobe, experimental petrology, MORB, abyssal peridotite, MELTS

INTRODUCTION

Basalts and peridotites convey information about the chemical activity of oxygen in the Earth's mantle, commonly expressed through the thermodynamic variable oxygen fugacity (f_{O_2}). Oxygen fugacity is important for understanding solubility and speciation of redox-sensitive volatile elements in mid-ocean ridge basalt (MORB) magmas and for anchoring extrapolation of the f_{O_2} -depth profile through Earth's upper mantle (Stagno and Frost 2010; Stagno et al. 2013) with consequences for the

depth of melting (Dasgupta et al. 2013) and the depth of metal saturation (O'Neill and Wall 1987; Ballhaus 1995; Rohrbach et al. 2011).

Mineral equilibria in abyssal peridotites dredged from the mid-ocean ridge system and Fe³⁺/ΣFe ratios of MORB glasses record information about f_{O_2} conditions in the sub-ridge mantle. These two sources of f_{O_2} information are independent; they rely on different samples, different thermodynamic f_{O_2} models, and different analytical techniques. Because some geochemical and geophysical inferences about the Earth depend on the absolute value of mantle f_{O_2} , for example, the depth to the diamond/graphite to carbonated melt reaction (Stagno et al. 2013), it is

* E-mail: fdavis@d.umn.edu

useful to consider the extent to which these two independent mantle f_{O_2} proxies agree. In this contribution, we compare results from the seminal study of Bryndzia and Wood (1990) on the f_{O_2} of abyssal peridotites, to results from (Zhang et al. 2018), which updates the study of Cottrell and Kelley (2011) on the f_{O_2} of MORB. The two global data sets do not appear to be in agreement about prevailing f_{O_2} conditions in the MORB source. Abyssal peridotites record a mean $\log f_{O_2}$ 0.9 log units below the quartz-fayalite-magnetite buffer (QFM-0.9 \pm 0.7) and a range from QFM-2.5 to QFM+0.5 (Bryndzia and Wood 1990), while MORB glasses record a mean of QFM-0.18 \pm 0.16 and range from QFM-0.7 to QFM+0.3 (Cottrell and Kelley 2011; Zhang et al. 2018). Frost and McCammon (2008) previously reported the \sim 1 log unit offset in f_{O_2} between abyssal peridotite and MORB. The apparent incongruence between melt-based and residue-based oxybarometers in nature indicates that our understanding of peridotite+melt assemblages as a function of f_{O_2} is nascent. The limited geographic distribution of peridotites, or the fact that peridotites and basalts from the same ridge segment have not been analyzed, may lead to sampling bias. It may be too that the assumption that these rocks are genetically related could be incorrect (e.g., Rampone et al. 1998). Or, the incongruence may result from a systematic offset between the two independent oxybarometers used to assess f_{O_2} : Bryndzia and Wood (1990) applied spinel oxybarometry to abyssal peridotites; Zhang et al. (2018) calculated f_{O_2} from silicate melt Fe^{3+}/Fe^{2+} ratios determined by Fe K-edge X-ray absorption near-edge structure (XANES) spectroscopy (Cottrell and Kelley 2011) via the algorithm of Kress and Carmichael (1991). We address this final possibility in this contribution.

In this paper, we report laboratory experiments that equilibrate basaltic-andesite melts with a solid assemblage of olivine+orthopyroxene+spinel over a range of f_{O_2} . We analyzed resulting spinel $Fe^{3+}/\Sigma Fe$ ratios by electron probe microanalysis (EPMA) using Mössbauer-characterized spinel standards for data-correction (Wood and Virgo 1989; Davis et al. 2017) and glass $Fe^{3+}/\Sigma Fe$ ratios by XANES (Cottrell et al. 2009; Zhang et al. 2018). These experiments allowed us to examine the chemistry of peridotite plus melt in a system with known, externally imposed f_{O_2} . Importantly, we are able to explore how the compositions of spinels in equilibrium with peridotite change with f_{O_2} . We compare these changes with three popular thermodynamic models for spinel and reveal broad consequences for melt generation in the upper mantle.

METHODS

Experimental methods

We made two starting materials intended to generate an equilibrium assemblage of olivine, orthopyroxene, spinel, and basaltic melt. The first starting material, "LOOS," produced run products with tiny spinel grains that made it difficult to find crystal-free glass pools for microanalysis. As a result, we present only a single experiment with this first starting material. We modeled starting mix "LOOS" on the run products of experiment 85-41c#4 from (Grove et al. 2003), which is one of only 20 experiments in the Library of Experimental Phase Relations (Hirschmann et al. 2008) saturated in all of these phases at 0.1 MPa.

We made two minor adjustments to the phase compositions before determining the bulk composition of the starting material. The glass in 85-41c#4 has 56.8 wt% SiO_2 , which is higher than the SiO_2 concentration range (48.06–52.91 wt%) of the experimental and natural basalts used by Cottrell et al. (2009), Cottrell and Kelley (2011), and Zhang et al. (2018) to demonstrate comparability of $Fe^{3+}/\Sigma Fe$ ratios in glasses determined by XANES to $Fe^{3+}/\Sigma Fe$ ratios determined by wet-chemical

analysis and Mössbauer spectrometry. We attempted to bring the composition of our experimental glasses closer to the SiO_2 range of MORB by increasing the concentration of TiO_2 in the melt component to 3 wt%, just outside the range of TiO_2 concentrations in the Cottrell and Kelley group's glasses (0.62–2.56 wt%). Addition of this amount of TiO_2 is expected to diminish SiO_2 of a liquid saturated in olivine and orthopyroxene by about 1 wt% (Xirouchakis et al. 2001). Because spinel also dissolves appreciable TiO_2 , we also added TiO_2 to the spinel component in an amount suggested by the experiment spinel/melt partition coefficient defined by the phases in 85-41c#4. After making these modifications to the phase components we calculated a bulk composition with the following proportions by weight: 70% melt, 10% olivine, 10% Opx, and 10% Spl.

We generated starting material LOOS2, which includes less of the spinel component, in an attempt to counteract abundant nucleation of spinel crystals. The bulk composition for LOOS2 was calculated with the following proportions by weight: 72% melt, 10% olivine, 15% Opx, and 3% Spl.

We mixed each of the starting materials from reagent oxide powders of SiO_2 , TiO_2 , Al_2O_3 , Cr_2O_3 , MgO , $MnCO_3$, Fe_2O_3 , $CaCO_3$, Na_2CO_3 , K_2CO_3 , and V_2O_5 . We fired most of these powders before mixing to remove surface adsorbed water for the following times and temperatures: SiO_2 at 1250 °C for 8 h; Al_2O_3 and MgO at 1200 °C for 88 h; TiO_2 at 1000 °C for 16 h; $CaCO_3$, Na_2CO_3 , and K_2CO_3 at 400 °C for 4, 12, and 8 h, respectively. We weighed all oxides except Cr_2O_3 and Fe_2O_3 and ground them in an agate mortar under ethanol for about 1 h. This mixture was then decarbonated in air by ramping temperature at 100 °C/h to 1000 °C and dwelling for 12 h. Weight of powders after the decarbonation step indicated that all CO_2 was driven off the powder. We then added to the mixture Cr_2O_3 and Fe_2O_3 and ground the combined mixture in an agate mortar under ethanol for about one hour. The final powder was stored in a desiccator. The compositions of the starting mixtures are given in Table 1.

We performed the experiments in DelTech vertical-tube gas mixing furnaces at the Smithsonian Institution National Museum of Natural History. We controlled oxygen fugacity using a mixture of CO and CO_2 gases and monitored f_{O_2} during the experiment using a ZrO_2 -Pt oxygen sensor, referenced to O_2 gas. We calibrated the sensor against a gas mixture of 50% CO and 50% CO_2 . Log f_{O_2} was controlled to within \pm 0.05 log units, with the exception of experiment LOOS2_2A, which experienced anomalous fluctuations in EMF we describe below. Temperature inside the furnace tube was monitored using a PtRh thermocouple and controlled to within \pm 2 of 1225 °C. The hottest region of the furnace was mapped by moving the thermocouple through the hotspot. The thermocouple was calibrated against the melting point of Au wire. Experimental charges were hung from Pt-loops by mixing starting powders with polyvinyl alcohol and partially fusing in air at 1400 °C. Each Pt loop was pre-saturated in Fe by equilibrating with experimental starting powder at the run temperature and gas mix of each experiment for 16–48 h. After pre-saturation, run products were removed from the loops by soaking in hydrofluoric acid overnight. Pt loops were then reloaded with starting powder and hung in the furnace under the conditions given in Table 2. Experiments were rapidly quenched by dropping the loop into a water bath without exposing the samples or gas mix in the furnace to air. We mounted experiments in epoxy and cut in half. One side was polished for electron microprobe analysis. The other half was double-side polished for analysis by XANES.

Experiment LOOS2_2A was held at an f_{O_2} of QFM+2.23 \pm 0.05 for the first 69 h of the run, but upon checking the EMF before quench, furnace f_{O_2} was found

TABLE 1. Compositions of experimental starting materials and model phase components as wt% oxides

	Starting materials		Phases from 85-41c#4 (Grove et al. 2003)				Modified melt and spinel components	
	LOOS	LOOS2	Glass	OI	Opx	Spl	Melt	Spl
SiO_2	48.72	52.67	56.8	39.4	56.4	0.18	55.78	0.18
TiO_2	2.25	2.20	0.93	0.02	0.09	0.43	3.00	1.39
Al_2O_3	12.70	11.77	15.6	0.05	1.18	18.1	15.36	18.11
Cr_2O_3	4.93	1.59	0.06	0.03	0.61	48.2	0.06	48.22
FeO^*	8.20	7.38	6.71	11.5	6.26	17.8	6.61	17.81
MnO	0.09	0.09	0.07	0.17	0.13	0.1	0.07	0.10
MgO	14.26	15.10	6.89	47.8	32.8	14.1	6.78	14.10
CaO	6.06	6.28	8.48	0.28	1.68	0.1	8.35	0.10
Na_2O	2.30	2.36	3.33				3.28	
K_2O	0.50	0.51	0.73				0.72	
P_2O_5			0.15					
NiO				0.18				
V_2O_5		0.05						
Total	100.00	100.00	99.75	99.43	99.15	99.01	100.00	100.00

TABLE 2. List of experimental details for 1 atm experiments at 1225 °C

Experiment name	Starting mix	Furnace $\log f_{\text{O}_2}^a$	$\log f_{\text{O}_2}$ (ΔQFM^b)	Duration (h)	Phase proportions (wt%)				Fe loss (% of ΣFe)	$\log f_{\text{O}_2}$ Spl-oxymetry	Error	$\log f_{\text{O}_2}$ XANES ^c
					Glass	OI	Opx	Spl				
LOOS2_-2A	LOOS2	-9.89	-1.87	70	76.1 (19)	12.5 (8)	8.7 (11)	2.8 (1)	18.7 (22)	-9.60	+0.47, -0.51	-9.72
LOOS2_-1B	LOOS2	-9.06	-1.04	73	75.4 (33)	11.0 (13)	10.7 (19)	2.9 (3)	6.5 (44)	-9.17	± 0.64	-9.26
LOOS2_-0.5A	LOOS2	-8.51	-0.49	72	74.6 (19)	7.7 (7)	14.7 (11)	2.9 (2)	10.6 (24)	-8.54	± 0.34	-8.78
LOOS_0B	LOOS	-8.13	-0.11	40	72.6 (30)	5.9 (12)	11.2 (18)	10.4 (5)	8.4 (40)	-8.81	+0.35, -0.38	-8.59
LOOS2_0.5A	LOOS2	-7.32	0.70	71	74.2 (19)	6.2 (7)	16.6 (11)	3.0 (2)	6.5 (26)	-7.62	± 0.32	-7.81
LOOS2_1B	LOOS2	-7.35	0.67	65	75.1 (20)	8.6 (8)	13.3 (12)	3.0 (2)	9.6 (26)	-7.39	+0.25, -0.26	-8.14
LOOS2_1.5A	LOOS2	-6.62	1.40	72	75.4 (18)	6.2 (7)	15.3 (10)	3.1 (2)	8.9 (23)	-7.11	± 0.20	-7.00
LOOS2_2A	LOOS2	-5.79 ^d	2.23	71	75.7 (19)	6.3 (7)	14.8 (11)	3.2 (2)	6.5 (25)	-6.20	+0.42, -0.40	-5.19

^a f_{O_2} in all instances is calculated in log bars.

^b Formulation of Frost (1991).

^c Standard error of $\log f_{\text{O}_2}$ by XANES is ± 0.64 log units following the standard error given in Kress and Carmichael (1988).

^d Some fluctuation in the furnace EMF were recorded in the final 2 h of this experiment, see text for details.

to be fluctuating anomalously at $\text{QFM}+2.36 \pm 0.15$. These fluctuations may have been occurring for as long as the last 2 h of the run. We have accounted for this fluctuation by presenting a larger uncertainty in furnace f_{O_2} for this experiment.

Electron microprobe analysis

Electron imaging (Fig. 1) was performed using a JEOL JXA-8530F Hyperprobe field-emission gun electron microprobe at the Smithsonian Institution. Glasses and minerals were analyzed for major elements by electron microprobe at the Smithsonian Institution using a JEOL 8900 Superprobe with five wavelength-dispersive spectrometers (WDS). We analyzed the $K\alpha$ peaks of the following elements: SiO_2 , TiO_2 , Al_2O_3 , Cr_2O_3 , FeO^* (ΣFe calculated as FeO), MnO , MgO , CaO , Na_2O , and K_2O . Glasses, olivines, and orthopyroxenes were analyzed using an accelerating voltage of 15 kV. Spinels were analyzed using an accelerating voltage of 13 kV in an attempt to excite a smaller volume, except spinels from LOOS_0B, which were analyzed with a 15 kV accelerating voltage. We analyzed glasses with a 10 μm diameter defocused spot and a 10 nA beam current. We analyzed minerals with a focused beam ($\sim 1 \mu\text{m}$ dia.) and beam current of 40 nA, except olivines from LOOS_0B, which were analyzed with a 15 nA beam current. We used the Armstrong/Love-Scott ZAF procedure for matrix correction (Armstrong 1988). Because orthopyroxene and spinel grains were small ($< 5 \mu\text{m}$ diameter), only one analytical point was collected for any given grain. Olivines were much larger, which allowed analysis of 3–5 points per grain on 3–5 total grains. Supplemental¹ Table 1 provides information on our primary standards, count times, and detector crystals. We selected peak positions for each element at the beginning of each analytical session by performing a wavelength scan in the region of the peak. We counted both peaks and backgrounds at each analytical point (Supplemental¹ Table 1).

Spinel crystals were so small (largest $< 3 \mu\text{m}$ across) that, even when analyzing at 13 kV, surrounding silicate glass was commonly sampled in the excitation volume. We analyzed only spinel crystals surrounded by glass and none that were partially or wholly included in olivine crystals. Resulting analyses were mixtures of varying proportions of spinel and glass compositions. We were able to remove analyses significantly sampling glass by discarding individual analyses that had Na_2O concentrations ≥ 0.05 wt%. Davis et al. (2017) found that Na_2O was not present above the limit of detection (~ 0.01 wt% under these analytical conditions) in any of the spinels analyzed in that study, so we expect that the actual Na_2O concentrations in spinels are negligible. After removing these obviously glass influenced analyses we still found that SiO_2 and CaO concentrations in the spinel were much higher ($\text{SiO}_2 > 0.5$ wt%; $\text{CaO} > 0.2$ wt%) than have been observed in many studies of natural spinels that report concentrations for these oxides ($\text{SiO}_2 < 0.2$ wt%, Canil et al. 1990; Ionov and Wood 1992; Woodland et al. 1992; Luhr and Aranda-Gómez 1997; Brunelli et al. 2006; Warren and Shimizu 2010; $\text{CaO} < 0.05$ wt%, Canil et al. 1990; Parkinson and Pearce 1998; Davis et al. 2017); although, there are a few examples where higher SiO_2 has been reported (SiO_2 between 0.7 and 1.5 wt%, Johnson and Dick 1992; Parkinson and Pearce 1998). Spinel from experiment 85-41c#4 of Grove et al. (2003), upon which our experimental starting material was based and generated under similar experimental conditions, was reported to have $\text{SiO}_2 = 0.18 \pm 0.37$ wt% and $\text{CaO} = 0.10 \pm 0.005$ wt%, further suggesting our observed high SiO_2 and CaO concentrations are anomalous. We attribute this excess SiO_2 and CaO in the analysis to secondary fluorescence of the surrounding glass. Secondary fluorescence of elements in low abundance is commonly observed in analyses of minerals included in a matrix with elevated abundances of those elements (e.g., Bastin et al. 1983; Llovet et al. 2000), and is likely an unavoidable consequence

of analyzing experimental spinels $< 3 \mu\text{m}$ in size using electron beam methods. Because excess SiO_2 and CaO in the spinel analysis can have a large effect on calculated $\text{Fe}^{3+}/\Sigma\text{Fe}$ ratios, especially if secondary fluorescence contributions from the two are not equal in magnitude, and because SiO_2 and CaO concentrations in these spinels are expected to be low, we have chosen to omit SiO_2 and CaO from our stoichiometric calculations of spinel $\text{Fe}^{3+}/\Sigma\text{Fe}$ ratios (Supplemental¹ Table 2, calculations described below). Full EPMA analyses of spinels including SiO_2 , CaO , and Na_2O are given in Supplemental¹ Table 3.

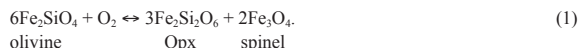
$\text{Fe}^{3+}/\Sigma\text{Fe}$ ratios in spinels were determined from the electron microprobe analyses following the method of Davis et al. (2017), which is a modification of the method presented by Wood and Virgo (1989). $\text{Fe}^{3+}/\Sigma\text{Fe}$ ratios of each spinel were calculated from spinel stoichiometry by normalizing the spinel cation proportions to 3 total cations, initially treating all Fe as Fe^{2+} , and then adjusting the $\text{Fe}^{3+}/\text{Fe}^{2+}$ ratio to balance the charge deficiency or excess (Stormer 1983). These initial estimates of $\text{Fe}^{3+}/\Sigma\text{Fe}$ ratios were then corrected by comparison to a set of spinel standards with $\text{Fe}^{3+}/\Sigma\text{Fe}$ ratios previously determined by Mössbauer spectrometry (Wood and Virgo 1989; Bryndzia and Wood 1990; Ionov and Wood 1992). The correction standards were analyzed at the beginning and end of each analytical session and a linear correction was defined by the relationship between $\text{Cr}\#$ ($\text{Cr}/[\text{Cr}+\text{Al}]$) and the difference between $\text{Fe}^{3+}/\Sigma\text{Fe}$ ratio determined by Mössbauer and by electron microprobe ($\Delta\text{Fe}^{3+}/\Sigma\text{Fe}^{\text{Möss-EPMA}}$). The correction was applied to all analyses of the experimental spinels irrespective of whether $\text{Cr}\#$ and $\Delta\text{Fe}^{3+}/\Sigma\text{Fe}^{\text{Möss-EPMA}}$ of the correction standards were found to be correlated (see discussion in Davis et al. 2017). Complete analyses of correction standards are given in Supplemental¹ Table 4.

X-ray absorption near-edge structure (XANES) analysis of $\text{Fe}^{3+}/\Sigma\text{Fe}$ ratios in glasses

We measured $\text{Fe}^{3+}/\Sigma\text{Fe}$ ratios in experimental glasses using XANES at bending magnet beamline X26A at the National Synchrotron Light Source, Brookhaven National Laboratory, U.S.A., following the method and basalt glass standards of (Cottrell et al. 2009). Before XANES analysis, the section of each experiment intended for XANES was double-polished to optical transparency ($< 100 \mu\text{m}$), and epoxy was removed by bathing in acetone. Reference glass LW_0 was analyzed to correct for energy drift related to the thermal load on the Si (311) monochromator (Cottrell et al. 2009). We evaluated the spectra for crystal interference (Supplemental¹ Fig. 1), and discarded spectra with evidence for crystal interference. The photon flux density at X26A was 6×10^7 photons/ μm^2 . Synchrotron radiation, at photon flux densities at least as high as 1×10^{13} photons/ $\text{s}/\mu\text{m}^2$, does not cause beam damage (oxidation or reduction) to Fe in anhydrous glasses (Cottrell et al. 2018). $\text{Fe}^{3+}/\Sigma\text{Fe}$ ratios in the glass were calculated from the drift-corrected centroids (area-weighted average energy of the pre-edge doublet in the XANES spectra) collected from the glasses according to the method of Cottrell et al. (2009), using the basalt calibration curve of Zhang et al. (2018). The Zhang et al. (2018) calibration accounts for the recoilless fraction in the Mössbauer spectra used to determine the $\text{Fe}^{3+}/\Sigma\text{Fe}$ ratios of the glass standards, making the Fe XANES measurements more accurate without sacrificing precision. We analyzed three independent points on each glass; we report our precision for the centroids and $\text{Fe}^{3+}/\Sigma\text{Fe}$ ratios of experimental glasses in Supplemental¹ Table 5. This reflects sample-specific reproducibility and encompasses any sample heterogeneity. Instrumental precision on the centroid of basalt glass standard AII_-05 (Cottrell et al. 2009) is ± 0.004 eV. Root mean square uncertainty on $\text{Fe}^{3+}/\Sigma\text{Fe}$ ratios predicted by our basalt calibration for unknowns is ± 0.01 (Zhang et al. 2018). XANES spectra are shown in Supplemental¹ Figure 2.

Calculation of oxygen fugacity

We calculated f_{O_2} recorded by the experimental run products from the chemical compositions of olivine, orthopyroxene, and spinel and, independently, from the $Fe^{3+}/\Sigma Fe$ ratio of the glass. For the mineral assemblage, f_{O_2} can be calculated from the following equilibrium:



We calculated f_{O_2} in bars using the following equation from Davis et al. (2017), which was derived from equations presented in Mattioli and Wood (1988) and Wood and Virgo (1989):

$$\log(f_{O_2})_{PT} = \frac{-24222}{T} + 8.64 + \frac{0.0567P}{T} - 12 \log(1 - Mg\#^{Ol}) - \frac{2620}{T} (Mg\#^{Ol})^2 + 3 \log(X_{Fe}^{M1} \cdot X_{Fe}^{M2})^{Opx} + 2 \log(a_{Fe_3O_4}^{sp}) \quad (2)$$

We used the same procedures to calculate each compositional variable in this equation as in Davis et al. (2017). We calculated f_{O_2} recorded by the $Fe^{3+}/\Sigma Fe$ ratio of the glass using equation 6 from Kress and Carmichael (1991). When we compare $\log f_{O_2}$ to the QFM buffer we use the formulation of Frost (1991).

Spinel compositional modeling

Several models can predict spinel compositions given an equilibrium melt composition. We have generated model spinel compositions for comparison with our experimental results using MELTS (Ghiorso and Sack 1995), SPINMELT (Ariskin and Nikolaev 1996), and MELT-CHROMITE (Poustovetov and Roeder 2001). We modeled spinel compositions in MELTS through the alphaMELTS application (Asimow and Ghiorso 1998; Smith and Asimow 2005). For each experiment, we input the composition of the glass measured by electron microprobe with all Fe as FeO, initialized the system at 0.1 MPa and 1225 °C, and held f_{O_2} constant at the value measured in the furnace. We initialized the phase equilibria at 1225 °C and then ran an isobaric, closed system (batch crystallization) cooling path to 1200 °C at temperature increments of 1 °C.

SPINMELT is not available as a stand-alone program and the corresponding author could not be reached. Our attempts to code SPINMELT from the information supplied in Ariskin and Nikolaev (1996) did not reproduce the results given in that paper, so we ran SPINMELT through PETROLOG 3.1.1.3 (Danyushevsky and Plechov 2011). In Petrolog 3, we performed crystallization runs with spinel as the only crystallizing phase and Ariskin and Nikolaev (1996) selected as the spinel compositional model. We set P to 0.1 MPa and f_{O_2} to the value measured in the furnace. We selected Kress and Carmichael (1988) as the melt Fe^{3+}/Fe^{2+} model and set fractionation of spinel to 0%. For each experiment we input the composition of the glass measured by electron microprobe with all Fe as FeO.

MELT-CHROMITE predicts a spinel composition in terms of five compositional components if given a melt composition, temperature, and pressure; it does this by simultaneously solving four empirically derived equations for compositional variables in the melt (Poustovetov and Roeder 2001). We solved these four equations in Microsoft Excel using the Solver add-in (Evolutionary mode) to minimize the sum of square residuals between the melt compositions and the equation outputs. We input glass compositions measured by electron microprobe with all FeO and Fe_2O_3 as determined by XANES, temperature of 1225 °C, and pressure of 0.1 MPa.

RESULTS

Melt and mineral phase textures, compositions, and modal proportions

Each experiment produced an assemblage of olivine, orthopyroxene, Cr-rich spinel, and basaltic glass (Fig. 1). Olivines formed euhedral crystals typically 40–60 μm across in the shortest direction. Orthopyroxenes formed small elongate grains <10 μm in width and <30 μm in length. Olivines and orthopyroxenes have quench rims (<300 nm) but show no evidence of large-scale chemical zonation. Spinel formed small grains <3 μm across.

Spinel compositions vary considerably with increasing f_{O_2} . It is most convenient to examine spinel compositions in terms

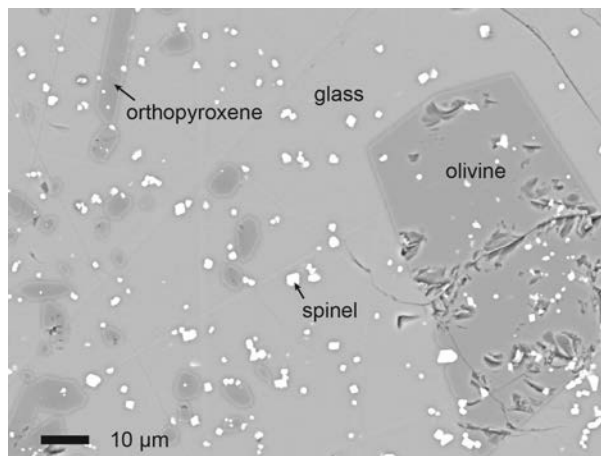


FIGURE 1. Backscattered electron image of sample LOOS2_1.5A showing typical sizes and textures of crystals grown in this study. Analysis of spinels by electron microprobe was particularly challenging given the small size of these crystals.

of major cations separated by stoichiometric units because it allows us to see which trivalent cations are substituting for Fe^{3+} as experimental f_{O_2} varies. Spinel has the general formula AB_2O_4 , where generally, A-type cations are divalent and B-type cations are trivalent; although, the ulvöspinel end-member ($TiFe_2O_4$) has Ti^{4+} as the A cation and Fe^{2+} as the B cation. After calculating spinel compositions per three total cations as described in Methods, a portion of the Fe^{2+} cations equal to two times the concentration of Ti cations was allocated to the B cations, and the remaining Fe^{2+} is allocated to the A cations. All Ti and Mg were assigned to A, and all Al, Cr, and Fe^{3+} were assigned to B.

Spinel compositions are presented in Supplemental¹ Table 2 in wt% oxides and in Figure 2 in units of cations per three total cations. Spinel A-type cations show little variation between QFM-1.87 and QFM+1.40 (Fig. 2a). Above QFM+1.40, Mg concentration increases, while Fe^{2+} decreases, consistent with the increase in Mg# observed in the coexisting liquid and olivine in that experiment (described below). Ti also decreases above QFM+1.40. Fe^{3+} increases as a proportion of the B-type cations as $\log f_{O_2}$ increases (Fig. 2b). This increase is approximately linear below QFM+1, but at higher f_{O_2} , more Fe^{3+} enters spinel per log unit increase in f_{O_2} . Cr concentration decreases linearly with increasing $\log f_{O_2}$ ($R^2 = 0.63$, p-value = 0.019), Al remains roughly constant from QFM-1.87 to QFM-0.11, but begins to decrease in concentration at $f_{O_2} > QFM$, and Fe^{2+} , which is tied to Ti in our calculation, remains constant from QFM-1.87 to QFM+1.40, decreasing only in the most oxidized experiment.

Several oxides in the glasses vary systematically with f_{O_2} (Fig. 3 and Supplemental¹ Table 5). SiO_2 ($R^2 = 0.77$, p-value = 0.004), TiO_2 ($R^2 = 0.76$, p-value = 0.005), Al_2O_3 ($R^2 = 0.71$, p-value = 0.009) all decrease in the melt with increasing f_{O_2} , while Fe_2O_3 ($R^2 = 0.79$, p-value = 0.003) increases. Cr_2O_3 concentrations in the glass from experiment LOOS_0B, the only experiment run using the very Cr-rich LOOS starting mix (Table 1), is greater than Cr_2O_3 concentrations in melts from LOOS2 experiments. When only experiments run on LOOS2 are considered, Cr_2O_3 decreases systematically in the melt with

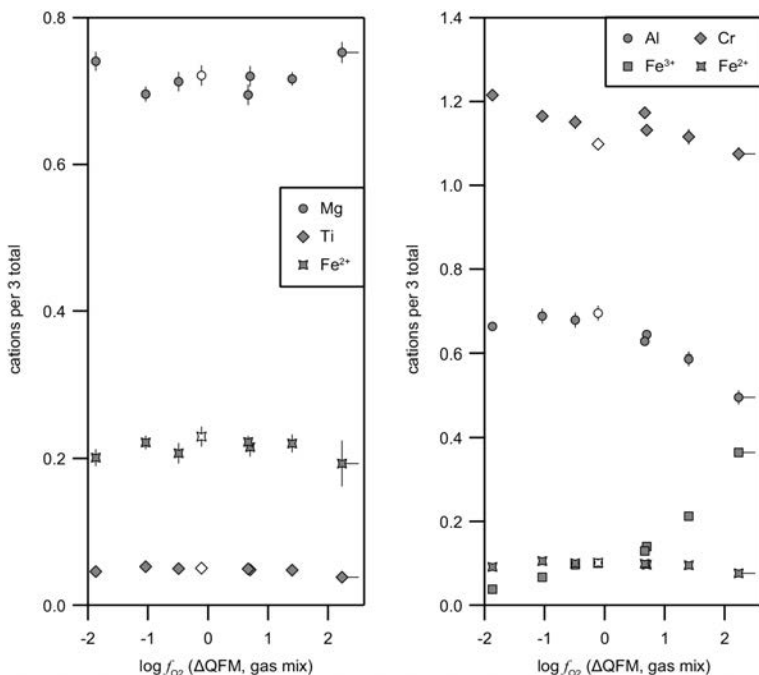


FIGURE 2. Molar cation compositions of experimental spinels normalized to three total formula cations. The x-axis shows $\log f_{O_2}$ (here and in subsequent figures f_{O_2} is in bars) relative to QFM as measured by the EMF of the oxygen sensor during the experiment. Error bars show error at 1σ . Where error bars are absent, uncertainty is less than the size of the data symbol. (a) A-type cations Mg, Ti, and Fe^{2+} . (b) B-type cations Al, Cr, Fe^{3+} , and Fe^{2+} associated with ulvöspinel component.

increasing f_{O_2} ($R^2 = 0.62$, p -value = 0.04). Other elements, notably the incompatible elements CaO, Na_2O , and K_2O , show no systematic variation with f_{O_2} .

Because all of the experiments are saturated in olivine and orthopyroxene of similar compositions, the activity of SiO_2 is nearly fixed. Therefore, decreasing SiO_2 with f_{O_2} in the glasses suggests a role for Fe^{3+} as a network former in these glasses. The relationship between SiO_2 in the melt and f_{O_2} observed in

these experiments suggests a significant fraction of Fe^{3+} may be tetrahedrally coordinated, consistent with studies of iron coordination in glass (e.g., Wilke et al. 2005). We observe a corresponding effect in the modal proportions of olivine and orthopyroxene, described below. On the other hand, we note that SiO_2 and Fe_2O_3 in the glass are not themselves significantly correlated ($R^2 = 0.42$, p -value = 0.08), therefore the causes of the correlation between SiO_2 and $\log f_{O_2}$ may be more complex than simple addition of Fe^{3+} to the melt.

With the exceptions of Mg# and Cr_2O_3 concentration, olivine (Supplementary¹ Table 6) and orthopyroxene (Supplementary¹ Table 7) compositions vary little with f_{O_2} . Given that the $Fe^{3+}/\Sigma Fe$ ratio of the liquid increases dramatically while total FeO increases only moderately, we expect that the Mg/ Fe^{2+} ratio of the melt, and therefore Mg# in the olivine, should increase with f_{O_2} . However, we do not observe a significant correlation between olivine Mg# and $\log f_{O_2}$ ($R^2 = 0.41$, p -value = 0.09, Fig. 4). It is likely that increasing f_{O_2} does lead to an increase in olivine Mg#, but the effect is obscured by Fe-loss from the system, which has affected the most reduced experiment to a greater degree (almost a factor of 2 greater) than the more oxidized experiments (Table 2). When we exclude the most reduced experiment (LOOS2_-2A) we find that Mg# in the remaining olivines does correlate with $\log f_{O_2}$ ($R^2 = 0.86$, p -value = 0.003). Mg# in this subset of the experiments increases about 0.005 per log unit increase in f_{O_2} (Fig. 4b), corresponding to an increase in Mg# of about 0.02 over the four orders of magnitude change in f_{O_2} that we explored in this study. A similar correlation between Mg# in orthopyroxene and $\log f_{O_2}$ is not observed.

Cr_2O_3 concentrations, as in the glass, generally decrease in olivine and orthopyroxene with increasing f_{O_2} . Again, Cr_2O_3 in both phases is highest in LOOS_0B, which used the higher Cr starting material. When we consider Cr_2O_3 from the perspective of mineral/melt partitioning, we find that olivine/melt and

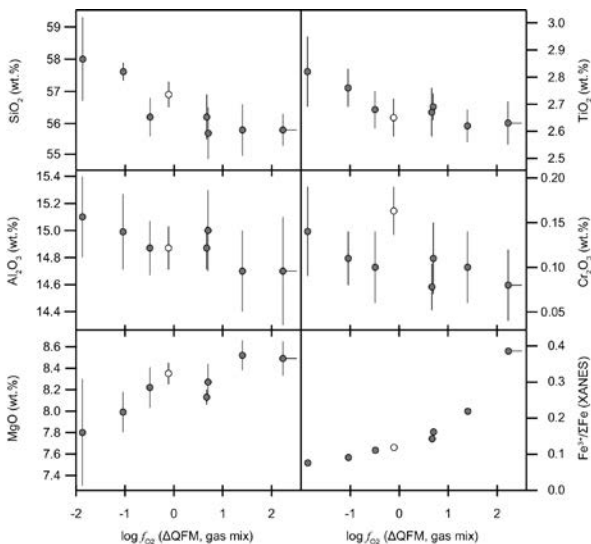


FIGURE 3. Major and minor element compositions of experimental glasses. White symbols indicate the composition of experiment LOOS_0B, which used the LOOS starting material. Gray symbols indicate glasses from experiments using the LOOS2 starting material. Error bars show error at 1σ . Where error bars are absent, uncertainty is less than the size of the data symbol.

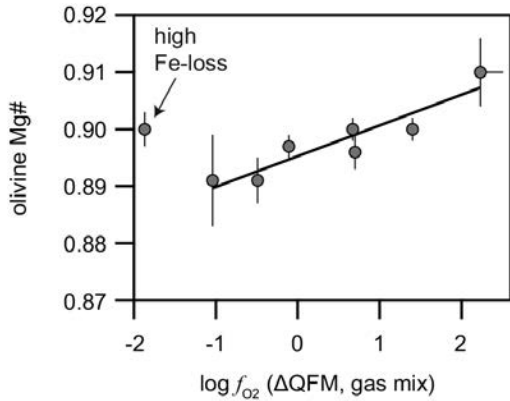


FIGURE 4. Mg# ($\text{Mg}/[\text{Mg}+\text{Fe}]$) of experimental olivines. Data symbols are as in Figure 3. (a) Olivine Mg# calculated directly from EPMA analysis. (b) Olivine Mg# corrected for the effects of Fe-loss, demonstrating the effect that changes in f_{O_2} would have on Mg# of olivine in an inert environment.

orthopyroxene/melt Cr partition coefficients are approximately constant ($D_{\text{Cr}}^{\text{ol}} = 1.3 \pm 0.2$ and $D_{\text{Cr}}^{\text{opx}} = 7.5 \pm 1.5$). This constant partitioning relationship suggests that most of the Cr is trivalent in our experiments, roughly consistent with the observations of Mallmann and O'Neill (2009) who observed a decrease in $D_{\text{Cr}}^{\text{opx}}$ at $f_{\text{O}_2} < \text{QFM}-1$. Our experiments do not extend to low enough f_{O_2} to make any further observations about Cr.

We calculated modal proportions of each phase by weight using multiple linear regression (Table 2, Fig. 5). The regression included a pure Fe phase to allow for an estimate of Fe-loss to the Pt loop. Phase proportions determined in this way always summed to between 99.7 and 99.9%. Modal proportions of phases were renormalized to exclude Fe lost to the Pt loop. Because one experiment uses the LOOS starting material, its modal phase proportions cannot be directly compared to those of the other experiments; therefore, we refer only to the phase proportions of the experiments from the LOOS2 series here. The percent of melt in the experiments is nearly constant over the range of f_{O_2} examined (Fig. 5a) with an average of $75.2 \pm 0.6\%$. Modal spinel increases with increasing $\log f_{\text{O}_2}$ (Fig. 5b). Although the absolute increase is small (2.8–3.2%) the correlation is significant ($R^2 = 0.96$, $p\text{-value} = 8 \times 10^{-5}$) and the change represents a 14% relative increase in modal spinel. Modal olivine decreases ($R^2 = 0.78$, $p\text{-value} = 0.009$) and modal orthopyroxene increases ($R^2 = 0.61$, $p\text{-value} = 0.04$) as $\log f_{\text{O}_2}$ increases, consistent with decreasing SiO_2 in the liquid as f_{O_2} increases.

Oxygen fugacities recorded by glasses and minerals

Calculations of f_{O_2} from the solid assemblage and from the $\text{Fe}^{3+}/\Sigma\text{Fe}$ ratios of the glasses are in agreement with the f_{O_2} of the gas mix monitored during the experiments and are in agreement with each other. We compare $\log f_{\text{O}_2}$ relative to QFM calculated from the solid assemblage to $\log f_{\text{O}_2}$ of the gas mix in Figure 6a. These independent assessments of system f_{O_2} are highly correlated ($R^2 = 0.96$, $p\text{-value} = 2 \times 10^{-5}$) with a slope near unity ($m = 0.85 \pm 0.07$) and a y-intercept near zero ($b = -0.19 \pm 0.09$). The average difference between $\log f_{\text{O}_2}$ of the furnace and $\log f_{\text{O}_2}$ calculated by Spl-oxybarometry is $-0.22 \pm$

0.31 log units, similar to the offset from furnace f_{O_2} observed in the experiments of Wood (1990). We compare $\log f_{\text{O}_2}$ calculated from the $\text{Fe}^{3+}/\Sigma\text{Fe}$ ratios of the glasses to $\log f_{\text{O}_2}$ of the gas mix in Figure 6b. These assessments of system f_{O_2} are similarly highly correlated ($R^2 = 0.91$, $p\text{-value} = 2 \times 10^{-4}$) and nearly coincide with a 1:1 line ($m = 1.03 \pm 0.13$ and $b = -0.23 \pm 0.17$). The

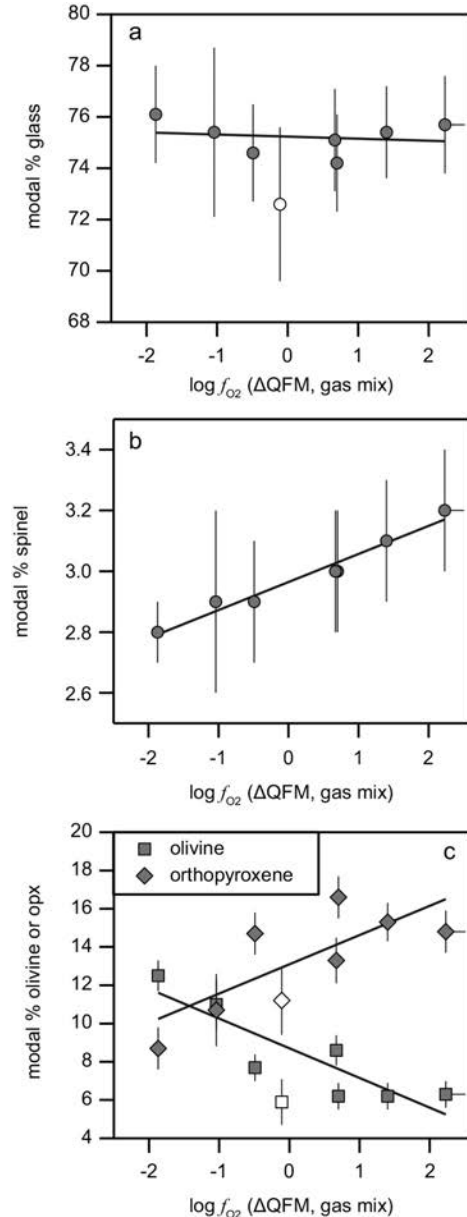


FIGURE 5. Modal proportions of phases (wt%) determined from mass balance. Symbol colors are as in Figure 3. Error bars show standard error of the multiple linear regression, propagated through renormalization after accounting for Fe-loss to the Pt loop. Bold black lines show linear regression of the modal proportions of each phase against $\log f_{\text{O}_2}$ (ΔQFM) calculated only from experiments using the LOOS2 starting material. (a) Modal proportion of glass. (b) Modal proportion of spinel. Experiment LOOS_0B not shown because it plots out of frame at a modal proportion of 10.4 ± 0.5 wt%. (c) Modal proportions of olivine and orthopyroxene.

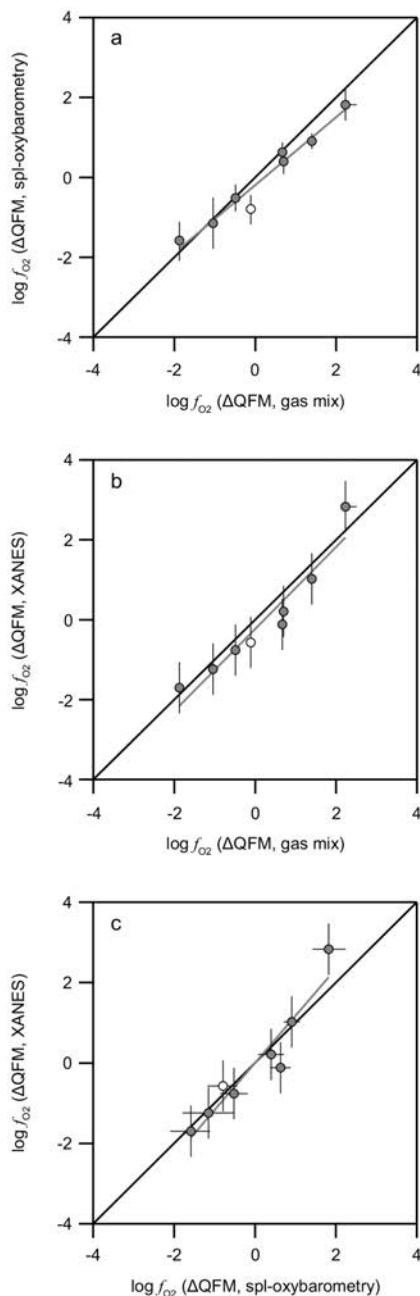


FIGURE 6. Comparisons of different methods of calculating f_{O_2} in the experiments. Error bars show 1σ errors. For XANES, 1σ errors were calculated from the standard error given by Kress and Carmichael (1988). Bold black line shows a 1:1 relationship between f_{O_2} calculated by each method being compared. Bold gray line shows the linear regression between methods of calculating f_{O_2} . See text for correlation coefficients, slopes, and intercepts of the regressions. (a) $\log f_{O_2}$ calculated from spinel oxybarometry plotted against $\log f_{O_2}$ measured in the experimental gas mix. (b) $\log f_{O_2}$ calculated from XANES measurement of $Fe^{3+}/\Sigma Fe$ in the glass plotted against $\log f_{O_2}$ measured in the experimental gas mix. (c) Comparison of $\log f_{O_2}$ calculated from Fe-XANES of the glass against $\log f_{O_2}$ calculated from spinel oxybarometry.

average difference between $\log f_{O_2}$ of the furnace and $\log f_{O_2}$ calculated from the glass $Fe^{3+}/\Sigma Fe$ ratios is -0.23 ± 0.43 log units. Glass from experiment LOOS2_2A records a notably higher f_{O_2} than the furnace environment, even as the mineral assemblage accurately records furnace f_{O_2} . It is possible that this offset is related to fluctuations in furnace f_{O_2} in the final 2 h of that experiment (described in Methods), which may have led to oxidation of the melt phase, but did not have time to be diffusively transmitted to the solids. We have also compared the two oxybarometers to each other (Fig. 6c), demonstrating their close agreement. Results of the two oxybarometers are correlated ($R^2 = 0.90$, p-value = 3×10^{-4}) and adhere closely to the 1:1 line ($m = 1.17 \pm 0.16$ and $b = 0.00 \pm 0.18$). Measurements of f_{O_2} from the two oxybarometers agree to within 1σ in all experiments.

Results of spinel compositional models

MELTS outputs predicted spinel to be a coexisting phase at 1225 °C in all but two of the model runs, and in each of the others spinel saturation was achieved by 1209 °C. MELTS also predicted orthopyroxene crystallization over this temperature interval in all runs and olivine saturation in two runs (Supplemental¹ Table 8). For each SPINMELT calculation run in Petrolog3, a temperature of spinel saturation and a spinel composition were output (Supplemental¹ Table 9). Four of the eight compositions gave saturation temperatures within ± 10 of 1225 °C. The other compositions gave spinel saturation temperatures $1269 < T < 1291$ °C, so differences in temperature between the experiments and the Petrolog output are expected to be minor. Compositions output by MELT-CHROMITE are in Supplemental¹ Table 10. Model spinel compositions are compared to experimental spinels in Figure 7. We discuss these model compositions below.

DISCUSSION

Using spinel peridotite oxybarometry and glass $Fe^{3+}/\Sigma Fe$ ratios from XANES to investigate f_{O_2} in Earth's upper mantle

Our experimental results suggest that when basaltic glasses and spinel peridotites are known to be in equilibrium, Fe-XANES of the glass and spinel oxybarometry give congruent results. Although the ranges of MORB-derived and peridotite-derived f_{O_2} overlap in nature, the mean f_{O_2} of the peridotite data set is significantly lower than the Zhang et al. (2018) basalt data set (t-test p-value $\ll 0.0001$; Fig. 8) or the wet-chemistry-derived Bézous and Humler (2005) data set (t-test p-value = 0.001). Our experimental results suggest that the incongruence between the $\log f_{O_2}$ records of MORB glasses and abyssal peridotites is not due to systematic differences between the two methods of determining $\log f_{O_2}$. Instead, these samples record real differences in $\log f_{O_2}$ at the time that the f_{O_2} records were frozen in.

Dependence of spinel compositions on f_{O_2}

Olivine, orthopyroxene, and melt compositions in these experiments vary little over 4 log units of f_{O_2} ; thus, the chemical variation we observe in the spinels reflects changes only in liquid $Fe^{3+}/\Sigma Fe$ ratios resulting from increasing f_{O_2} . Even the small systematic chemical variations observed in the other phases

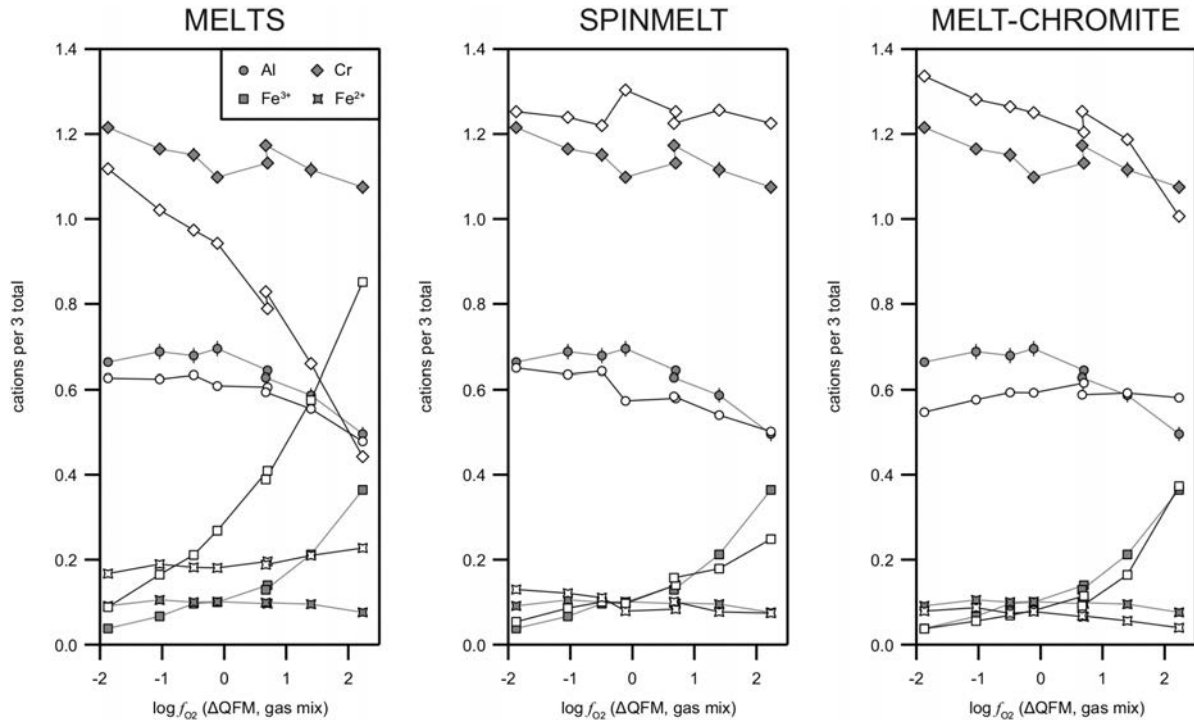


FIGURE 7. Comparison between experimental spinels from this study with model spinel compositions calculated from three different models. Compositions are presented as modal cations proportions per three total cations. Only B-type cations are shown. Gray symbols are experimental compositions from this study with error bars as in Figure 2. White symbols are model output spinel compositions. Gray and black tie lines are meant only to aid the reader in connecting data and model output series that cross or overlap one another. (a) Model results from MELTS (Ghiorso and Sack 1995), calculated using the alphaMELTS application (Asimow and Ghiorso 1998; Ghiorso et al. 2002; Smith and Asimow 2005). Additional details given in the text. (b) Model results from SPINMELT (Ariskin and Nikolaev 1996) calculated using Petrolog3 (Danyushevsky and Plechov 2011). Additional details given in text. (c) Model results from MELT-CHROMITE (Poustovetov and Roeder 2001).

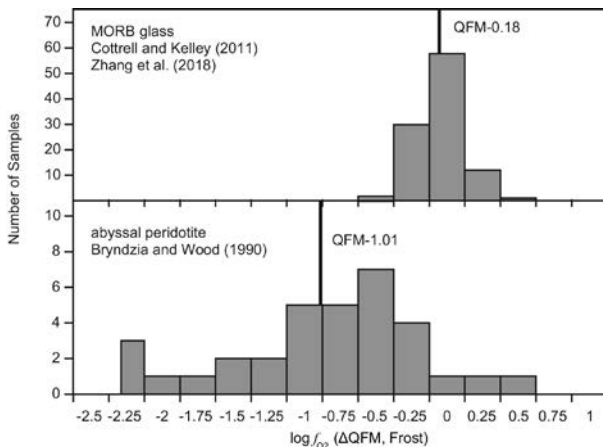


FIGURE 8. Histograms of f_{O_2} measurements from MORB (Cottrell and Kelley 2011; Zhang et al. 2018) and abyssal peridotites (Bryndzia and Wood 1990). All literature data has been reported relative to QFM following the formulation of Frost (1991). Consequently, averages are slightly different than reported in some of the original sources.

occur in a system with equilibrium olivine and orthopyroxene, and, therefore, reflect chemical changes to a peridotite-saturated system that are inextricable from changes in f_{O_2} . For example,

the ~2 wt% decrease in SiO_2 in the melt from the most reducing to the most oxidizing experiments reflects changes in the melt composition due to increased Fe^{3+} in the melt while activity of SiO_2 is held constant by equilibrium between olivine and orthopyroxene. These experimental spinels, then, can provide direct insights into how spinel compositions in spinel peridotites evolve as f_{O_2} of the system is perturbed at 0.1 MPa and constant temperature.

Our experimental study is unique in the sense that it examines compositional effects of f_{O_2} on a peridotite plus melt system over a range of f_{O_2} conditions comparable to those found in magmatic systems on Earth. As mentioned in Methods, there are only 20 experiments in the LEPR database with an assemblage of melt+olivine+orthopyroxene+spinel at 0.1 MPa and controlled f_{O_2} . Of those 20, 15 are from a single study by Barnes (1986) with f_{O_2} varying from QFM-3.81 to QFM+0.75 and temperatures from 1157 to 1323 °C. A comparison of our spinel compositions with the spinels from Barnes (1986) within ± 50 °C of our experimental temperature of 1225 °C shows close agreement over the range at which the experiments overlap. But the most interesting compositional changes we have observed occur at $f_{O_2} > QFM+1$ where Fe^{3+} begins to dilute the concentration of Al and Ti in the spinel in addition to Cr (Fig. 4), and there are no peridotite-saturated data for direct comparison under these conditions.

Ballhaus et al. (1991) performed peridotite-saturated experi-

ments over a range of f_{O_2} at pressures between 0.3 and 2.7 GPa using several different bulk compositions, but whether these experiments show similar compositional trends to what we have observed in this study is ambiguous. Spinels produced by the different starting materials at any given pressure in the Ballhaus et al. (1991) study variably show no change in Al in spinel with f_{O_2} (mix S1297 at 2.5 GPa), steadily decreasing Al with f_{O_2} (mix MPY30 at 1 GPa), or steady Al at low f_{O_2} and steep decreases in Al at higher f_{O_2} (mix MPY30 at 2.5 GPa). Comparison of these results with our experiments is complicated because temperature varies over a range >200 °C in most combinations of starting material and pressure, and only one of these combinations has a total number of experiments greater than 4. There are 6 experiments from Ballhaus et al. (1991) run using mix MPY30 at 2.5 GPa and within ± 50 °C of 1100 °C. These experiments produced spinel with an approximately constant Al concentration below QFM+3 as Fe^{3+} increased steadily, and then a steep decrease in Al at higher f_{O_2} , similar to what we observe in our 0.1 MPa experiments above QFM+1. There is clearly need for more experiments in peridotite saturated systems at a range of f_{O_2} and pressures to better define f_{O_2} dependence of spinel compositions.

We compare model spinel compositions from MELTS (Ghiorso and Sack 1995; Smith and Asimow 2005), SPINMELT (Ariskin and Nikolaev 1996), and MELT-CHROMITE (Poustovetov and Roeder 2001) to the compositions of experimental spinels from this study in Figure 7. We also modeled spinel compositions in pMELTS (Ghiorso et al. 2002), but resulting spinels were less accurate than MELTS output, and we do not discuss them further. There are two important aspects of the model outputs that we want to consider: (1) how accurately do the models reproduce the compositions of the experimental spinels, and (2) how well do the models predict changes in the exchange reactions between spinel and melt? The second question in particular is important for assessing how likely it is that a model will be able to predict conditions outside its calibration data set or how well the model will be able to predict behavior in a dynamic system.

The model spinels produced by MELTS are the least accurate of the three models considered; however, MELTS captures changes in the exchange reactions observed in the experiments that the other models do not. MELTS over-predicts the concentrations of Fe^{3+} (+0.05 to +0.49 cations per formula unit, pfu) and of the ulvöspinel component (+0.08 to +0.15 Fe^{2+} cations pfu), while under-predicting Cr concentration (−0.09 to −0.63 cations pfu). But MELTS captures the change in Al with f_{O_2} the best of the three models considered, both in accuracy for any given melt- f_{O_2} pair and in the overall topology of the curve (Fig. 7a). All model spinels produced by MELTS have Al concentrations within ± 0.09 cations per formula unit of the corresponding experimental spinel. Most importantly, MELTS predicts little change in Al concentrations at $f_{O_2} < QFM+0.5$ and decreasing Al at higher f_{O_2} , just as we observe in our experimental spinels. MELTS captures this change in the substitution mechanism for Fe^{3+} into spinel, replacing only Cr at f_{O_2} less than about QFM and replacing Al and Cr at higher f_{O_2} better than the other two models.

SPINMELT and MELT-CHROMITE are at least partly empirical, and while their overall accuracy in predicting spinel compositions is better than MELTS, they do not capture changes

in the cation exchange reactions seen the experiments. At f_{O_2} below QFM+2, SPINMELT accurately predicts the ulvöspinel component (within ± 0.02 Fe^{2+} cations pfu) and Fe^{3+} concentrations (within ± 0.09 cations pfu), but does not predict the high Fe^{3+} concentration of the most oxidizing experiment (Fig. 7b). SPINMELT also accommodates all of the Fe^{3+} increase with linearly decreasing Al, while Cr concentrations remain roughly constant. This leads to variable accuracy in predicting Al concentrations (−0.13 to +0.14 cations pfu) and consistent overestimation of Cr concentrations (+0.03 to +0.21 cations pfu). This contrasts with the decrease in Cr observed in our experiments. SPINMELT's inability to predict which trivalent cations will substitute for Fe^{3+} is consistent with the limited range of Cr/Al in the calibration data used to formulate SPINMELT (Ariskin and Nikolaev 1996; Poustovetov and Roeder 2001).

Of the models we examined, MELT-CHROMITE was most successful at accurately predicting Fe^{3+} concentrations (within ± 0.05 cations pfu), and although it consistently underestimated the ulvöspinel component, overall accuracy was good (−0.01 to −0.04 Fe^{2+} cations pfu). However, MELT-CHROMITE over-predicts Cr/Al ratios in experiments more reducing than QFM+2 and under-predicts Cr/Al ratios of the most oxidizing run. Importantly, MELT-CHROMITE predicts that spinel Al concentrations remain roughly constant as f_{O_2} increases, with all additional Fe^{3+} being accommodated by decreasing Cr concentrations. Instead, our experiments show that Fe^{3+} is accommodated by decreasing Cr and Al above QFM.

The comparison of the model results to our experiments highlights the need for additional experimental spinel compositions produced over a range of f_{O_2} to feed the next generation of spinel models. Although SPINMELT and MELT-CHROMITE are reasonably accurate, their inability to capture changes in the trivalent cation exchange reactions suggest that they will not perform well outside their calibration ranges (for example, at high pressures), nor will they be able to accurately predict changes to dynamic systems. Modeling near-fractional melting of peridotite in the upper mantle will require Cr, Al, and Fe^{3+} exchange be modeled accurately. Inaccuracies in how these cations exchange will be compounded over each melting step and will tend to move the bulk composition of the system away from the behavior of the natural system, even if any individual step produces relatively accurate spinel compositions.

Given the sophisticated nature of MELTS and the clear desire by the community to use it to model partial melting of the mantle (e.g., Hirschmann et al. 1999; Asimow et al. 2001; Coogan et al. 2004; Gaffney et al. 2005; Lambart et al. 2009; Byerly and Lassiter 2014), it is worth further investigating the inaccurate predictions by MELTS of Cr and Fe^{3+} concentrations in spinels at a given f_{O_2} . The extent of the problem can be demonstrated by comparing the activities of magnetite ($a_{Fe_3O_4}^{SpI}$) in experimental and model spinels (Fig. 9). We have calculated $a_{Fe_3O_4}^{SpI}$ of the spinels from our experiments and those spinel compositions output by MELTS using the MELTS Supplemental Calculator (Sack and Ghiorso 1991a, 1991b; <http://melts.ofm-research.org/CalcForms/index.html>). At a given f_{O_2} , MELTS predicts spinels with $a_{Fe_3O_4}^{SpI}$ 0.6 to 0.9 log units higher than in the spinels that are produced experimentally. Magnetite activity is the variable with the greatest leverage over the calculation of f_{O_2} from olivine-orthopyroxene-spinel equilibria,

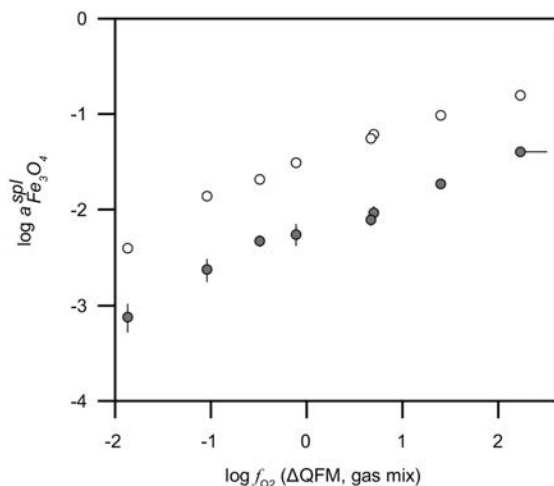


FIGURE 9. Log activities of magnetite in the experimental (gray) and MELTS model (white) spinels. Activities were calculated using the MELTS Supplemental Calculator (Sack and Ghiorso 1991a, 1991b; <http://melts.ofin-research.org/CalcForms/index.html>).

and it is difficult to reconcile this great a difference in $a_{\text{Fe}_3\text{O}_4}^{\text{Sp}}$ in spinels nominally recording the same f_{O_2} .

In two of our MELTS runs, the model predicted co-saturation of olivine, orthopyroxene, and spinel at temperatures between 1225 and 1200 °C, allowing us to independently calculate f_{O_2} from the output mineral compositions. We recalculated f_{O_2} of these model assemblages using the oxybarometer of Mattioli and Wood (1988) (Eq. 4 of Davis et al. 2017) and using the MELTS supplemental Calculator to calculate $a_{\text{Fe}_3\text{O}_4}^{\text{Sp}}$. The combination of this oxybarometer and method of calculating magnetite activity in spinel has been shown to accurately reproduce experimental f_{O_2} at 0.1 MPa (Wood 1990; Herd 2008; Davis et al. 2017). In each case, f_{O_2} calculated from the experimental mineral compositions accurately predicts the furnace f_{O_2} , but the MELTS model run predicts f_{O_2} that is ~ 1.2 log units too high (Supplemental¹ Table 8). This suggests that MELTS can produce a peridotite solid assemblage that is out of redox equilibrium with a coexisting liquid by greater than a log unit of f_{O_2} . AlphaMELTS provides an option that allows the system to calculate f_{O_2} from the solid assemblage rather than from the melt composition (ALTERNATIVE_FO2). We also ran alphaMELTS with ALTERNATIVE_FO2 turned on, and found that, although spinel Fe_2O_3 is slightly lower and Cr_2O_3 slightly higher than with this option turned off, there is negligible effect on calculated f_{O_2} (Supplemental¹ Table 8).

Experimental melt fraction and the limited solidus depression caused by Fe^{3+}

Given the expectation that Fe^{3+} should behave incompatibly during peridotite partial melting (Canil et al. 1994), it is notable that experimental melt fraction remains constant in the experimental series as the only bulk compositional change is in the ratio of $\text{Fe}_2\text{O}_3/\text{FeO}$ (Fig. 5a). It may be that the modest solidus depressing power of Fe^{3+} is partially offset by a corresponding increase in Mg# of olivine and orthopyroxene, but our data also demonstrate that Fe^{3+} becomes increasingly compatible in spinel as f_{O_2} increases (Fig. 10) and Fe^{3+} constitutes a greater propor-

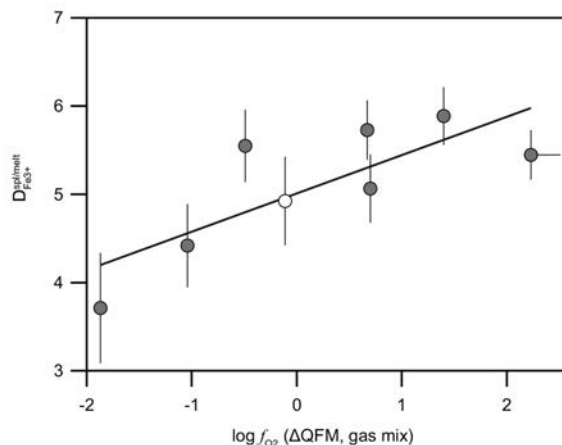


FIGURE 10. Effects of changing $\log f_{\text{O}_2}$ on spinel/melt partitioning of Fe^{3+} . Symbols are as in Figure 3, and error bars are at 1σ . The best-fit line has slope = 0.43 ± 0.14 , y-intercept = 5.01 ± 0.17 , and $R^2 = 0.62$ with p-value = 0.02.

tion of the B-type cations. The increasing compatibility of Fe^{3+} as the magnetite component in spinel increases is an important and interesting result of our study. At this time, we do not have enough information to say definitively why Fe^{3+} becomes more compatible in spinel as f_{O_2} increases, though we can speculate. It is likely that progressive changes in spinel chemistry lessen the mismatch between the ionic radius of Fe^{3+} and the lattice site in which it sits, creating more favorable site geometry for Fe^{3+} on the octahedral site, and possibly the tetrahedral site as well. It is beyond the scope of this paper to determine the site specificity of Fe^{3+} accommodation in spinel, but the increased compatibility of Fe^{3+} at constant melt fraction as f_{O_2} increases has important consequences for melting in Earth.

Instead of promoting melting, increasing bulk $\text{Fe}^{3+}/\Sigma\text{Fe}$ ratios in peridotites drive reactions analogous to the fayalite-ferrosilite-magnetite reaction (Eq. 1). Fe^{3+} may become less incompatible in bulk peridotite as it becomes more abundant by both increasing modal spinel and increasing the spinel/melt partition coefficient of Fe^{3+} —effectively cancelling any solidus-depressing capability that Fe^{3+} might otherwise have. If this interpretation is correct, then there is no reason to expect $\text{Fe}^{3+}/\Sigma\text{Fe}$ ratios of basalts to correlate with other incompatible elements once the effects of low-pressure fractionation are corrected for, which may partly explain the absence of correlation between Na_2O and Fe_2O_3 in fractionation-corrected MORB (Bézos and Humler 2005; Cottrell and Kelley 2011).

IMPLICATIONS

Our comparison between f_{O_2} calculated from olivine, orthopyroxene, and spinel mineral analyses by electron microprobe and f_{O_2} calculated from $\text{Fe}^{3+}/\Sigma\text{Fe}$ ratios of basaltic glasses measured by XANES demonstrates that these methods are both accurate and directly comparable. Focus must now shift to whether f_{O_2} recorded by peridotites and basalts drawn from the same tectonic settings can be corrected for the effects of petrological processes after separation of melts from peridotite residues to reveal f_{O_2} conditions in melting source regions. To a degree, this problem

has already been solved for mid-ocean ridge basalts (MORB). Decompression of a basaltic liquid as it rises from a magma chamber to the surface causes a small (~ 0.25 log unit), predictable change in f_{O_2} relative to quartz-fayalite-magnetite (QFM) (Kress and Carmichael 1991), and the effects of olivine fractionation on MORB $Fe^{3+}/\Sigma Fe$ ratios can also be corrected back to equilibrium with mantle olivine (Cottrell and Kelley 2011).

Correcting peridotite f_{O_2} back to magma source conditions is more complex. Peridotites from many different tectonic settings invariably record colder temperatures than magmatic conditions (e.g., Bryndzia and Wood 1990; Woodland et al. 1992; Nasir 1996; Parkinson and Arculus 1999). Simply recalculating f_{O_2} of a given spinel peridotite at higher temperatures leads to a decrease in f_{O_2} relative to QFM. Temperature enters into the f_{O_2} calculation directly and in the calculations of magnetite and fayalite activities; therefore, the effects of temperature are compositionally dependent, but may be as much as -0.2 log units relative to QFM per $100^\circ C$ (Davis et al. 2017). It is not sufficient to perform calculations at a hotter temperature without also accounting for metamorphic reactions that have occurred upon cooling. Canil and O'Neill (1996) suggested that as peridotites cool, spinel exsolves from pyroxenes, leading to dilution of the magnetite component. This effect should tend to lower f_{O_2} of the peridotite, counter to the effect of temperature on the calculation of f_{O_2} . Voigt and von der Handt (2011) developed a model for calculating changing Cr# and modal proportion of spinel in peridotites upon cooling, but the model does not take into account exchange of Fe^{3+} between spinel and pyroxenes. As we demonstrated, MELTS is not able to accurately predict spinel compositions at a given f_{O_2} , so there is currently no model available that can estimate the effects of metamorphic reactions in a cooling spinel peridotite on recorded f_{O_2} . There is a clear need for additional experimental constraints on spinel compositional variability in equilibrium with olivine and pyroxene across a range of f_{O_2} .

More accurate spinel compositional models are not only needed to reconcile the MORB and abyssal peridotite f_{O_2} data, but also to allow for reconstruction of mantle f_{O_2} conditions at depths equal to and greater than the region of MORB melting. How f_{O_2} changes as a function of depth in Earth's upper mantle affects phase stability (Stagno and Frost 2010; Rohrbach et al. 2011; Stagno et al. 2013) and rheological properties of the mantle (Keefner et al. 2011). MORB glasses and abyssal peridotites anchor that redox profile. Because spinel composition is the variable with the greatest leverage over the f_{O_2} recorded by the solids, accurate modeling of the evolution of spinel compositions during melt extraction are required for any forward model of mantle melting. Our MELTS modeling suggests that MELTS predicts residues that are too oxidized to have equilibrated with the coexisting liquid phase. It is not obvious how this would affect a multistep, fractional melting calculation in MELTS. On one hand, it may be that MELTS will produce a series of fractional melts that are each more reduced than should be produced from the equilibrium solid assemblage at any given step, this might lead MELTS to under-predict f_{O_2} in the aggregate melt. On the other hand, at any given step, the liquid is extracting too little Fe^{3+} from the residue, so the residue may evolve along a more oxidized trajectory than in nature. Thinking outside of MELTS, we can reasonably ask the questions: Is incompatible Fe^{3+} suc-

cessively depleted in peridotite residues as melts are extracted, leading to decreasing f_{O_2} relative to QFM as melting proceeds (e.g., Canil et al. 1994)? Or does Al- Fe^{3+} exchange between spinel and melt, which favors increasing spinel Fe^{3+}/Al ratios as melting proceeds (Ballhaus et al. 1991), lead to an increase, or perhaps no change, in the f_{O_2} of the mantle as melts are extracted? Our results suggest that the toolbox is not yet up to the job of answering these questions.

ACKNOWLEDGMENTS

We thank Suzanne Birner and Paul Asimow for helpful discussions. We acknowledge support from NSF OCE-1433212 and a Smithsonian National Museum of Natural History Peter Buck Fellowship to F.D. We are grateful for assistance from Tony Lanzirrotti, Sue Wirick, Tim Gooding, and Tim Rose. This paper was improved by constructive reviews from N. Métrich and an anonymous reviewer. We appreciated support of X26A from Department of Energy (DOE) GeoSciences DE-FG02-92ER14244. The DOE Office of Science supported use of the NSLS under Contract No. DE-AC02-98CH10886.

REFERENCES CITED

- Ariskin, A.A., and Nikolaev, G.S. (1996) An empirical model for the calculation of spinel-melt equilibria in mafic igneous systems at atmospheric pressure: 1. Chromian spinels. *Contributions to Mineralogy and Petrology*, 123, 282–292.
- Armstrong, J. (1988) Quantitative analysis of silicate and oxide minerals: comparison of Monte Carlo, ZAF and phi-rho-z procedures. *Microbeam Analysis*, 23, 239–246.
- Asimow, P.D., and Ghiorso, M.S. (1998) Algorithmic modifications extending MELTS to calculate subsolidus phase relations. *American Mineralogist*, 83, 1127–1132.
- Asimow, P.D., Hirschmann, M., and Stolper, E. (2001) Calculation of peridotite partial melting from thermodynamic models of minerals and melts, IV. Adiabatic decompression and the composition and mean properties of mid-ocean ridge basalts. *Journal of Petrology*, 42, 963–998.
- Ballhaus, C. (1995) Is the upper mantle metal-saturated? *Earth and Planetary Science Letters*, 132, 75–86.
- Ballhaus, C., Berry, R., and Green, D. (1991) High pressure experimental calibration of the olivine-orthopyroxene-spinel oxygen geobarometer: implications for the oxidation state of the upper mantle. *Contributions to Mineralogy and Petrology*, 107, 27–40.
- Barnes, S.J. (1986) The distribution of chromium among orthopyroxene, spinel and silicate liquid at atmospheric pressure. *Geochimica et Cosmochimica Acta*, 50, 1889–1909.
- Bastin, G., Van Loo, F., Vosters, P., and Vrolijk, J. (1983) A correction procedure for characteristic fluorescence encountered in microprobe analysis near phase boundaries. *Scanning*, 5, 172–183.
- Bézos, A., and Humler, E. (2005) The $Fe^{3+}/\Sigma Fe$ ratios of MORB glasses and their implications for mantle melting. *Geochimica et Cosmochimica Acta*, 69, 711–725.
- Brunelli, D., Seyler, M., Cipriani, A., Ottolini, L., and Bonatti, E. (2006) Discontinuous melt extraction and weak refertilization of mantle peridotites at the Vema lithospheric section (Mid-Atlantic Ridge). *Journal of Petrology*, 47, 745–771.
- Bryndzia, L.T., and Wood, B.J. (1990) Oxygen thermobarometry of abyssal spinel peridotites: the redox state and C–O–H volatile composition of the Earth's sub-oceanic upper mantle. *American Journal of Science*, 290, 1093–1116.
- Byerly, B.L., and Lassiter, J.C. (2014) Isotopically ultradepleted domains in the convecting upper mantle: Implications for MORB petrogenesis. *Geology*, 42, 203–206.
- Canil, D., and O'Neill, H.St.C. (1996) Distribution of ferric iron in some upper-mantle assemblages. *Journal of Petrology*, 37, 609–635.
- Canil, D., Virgo, D., and Scarfe, C.M. (1990) Oxidation state of mantle xenoliths from British Columbia, Canada. *Contributions to Mineralogy and Petrology*, 104, 453–462.
- Canil, D., O'Neill, H.St.C., Pearson, D., Rudnick, R., McDonough, W., and Carswell, D. (1994) Ferric iron in peridotites and mantle oxidation states. *Earth and Planetary Science Letters*, 123, 205–220.
- Coogan, L.A., Thompson, G., MacLeod, C.J., Dick, H., Edwards, S., Scheirer, A.H., and Barry, T.L. (2004) A combined basalt and peridotite perspective on 14 million years of melt generation at the Atlantis Bank segment of the Southwest Indian Ridge: evidence for temporal changes in mantle dynamics? *Chemical Geology*, 207, 13–30.
- Cottrell, E., and Kelley, K.A. (2011) The oxidation state of Fe in MORB glasses and the oxygen fugacity of the upper mantle. *Earth and Planetary Science Letters*, 305, 270–282.
- Cottrell, E., Kelley, K.A., Lanzirrotti, A., and Fischer, R.A. (2009) High-precision determination of iron oxidation state in silicate glasses using XANES. *Chemical Geology*, 268, 167–179.

- Cottrell, E., Lanzirotti, A., Mysen, B.O., Birner, S.K., Kelley, K.A., Botcharnikov, R., Davis, F.A., and Newville, M. (2018) A Mössbauer-based XANES calibration for hydrous basalt glasses reveals radiation-induced oxidation of Fe. *American Mineralogist*, 4, 489–501.
- Danyushevsky, L.V., and Plechov, P. (2011) Petrolog3: Integrated software for modeling crystallization processes. *Geochemistry, Geophysics, Geosystems*, 12.
- Dasgupta, R., Mallik, A., Tsuno, K., Withers, A.C., Hirth, G., and Hirschmann, M.M. (2013) Carbon-dioxide-rich silicate melt in the Earth's upper mantle. *Nature*, 493, 211–215.
- Davis, F.A., Cottrell, E., Birner, S.K., Warren, J.M., and Lopez, O.G. (2017) Revisiting the electron microprobe method of spinel-olivine-orthopyroxene oxybarometry applied to spinel peridotites. *American Mineralogist*, 102, 421–435.
- Frost, B.R. (1991) Introduction to oxygen fugacity and its petrologic importance. *Reviews in Mineralogy and Geochemistry*, 25, 1–9.
- Frost, D.J., and McCammon, C.A. (2008) The redox state of Earth's mantle. *Annual Review of Earth and Planetary Sciences*, 36, 389–420.
- Gaffney, A.M., Nelson, B.K., and Blichert-Toft, J. (2005) Melting in the Hawaiian plume at 1–2 Ma as recorded at Maui Nui: the role of eclogite, peridotite, and source mixing. *Geochemistry, Geophysics, Geosystems*, 6.
- Ghiorso, M.S., and Sack, R.O. (1995) Chemical mass transfer in magmatic processes IV. A revised and internally consistent thermodynamic model for the interpolation and extrapolation of liquid-solid equilibria in magmatic systems at elevated temperatures and pressures. *Contributions to Mineralogy and Petrology*, 119, 197–212.
- Ghiorso, M.S., Hirschmann, M.M., Reiners, P.W., and Kress, V.C. (2002) The pMELTS: A revision of MELTS for improved calculation of phase relations and major element partitioning related to partial melting of the mantle to 3 GPa. *Geochemistry, Geophysics, Geosystems*, 3, 1–35.
- Grove, T.L., Elkins-Tanton, L.T., Parman, S.W., Chatterjee, N., Müntener, O., and Gaetani, G.A. (2003) Fractional crystallization and mantle-melting controls on calc-alkaline differentiation trends. *Contributions to Mineralogy and Petrology*, 145, 515–533.
- Herd, C.D. (2008) Basalts as probes of planetary interior redox state. *Reviews in Mineralogy and Geochemistry*, 68, 527–553.
- Hirschmann, M., Asimow, P.D., Ghiorso, M., and Stolper, E. (1999) Calculation of peridotite partial melting from thermodynamic models of minerals and melts. III. Controls on isobaric melt production and the effect of water on melt production. *Journal of Petrology*, 40, 831–851.
- Hirschmann, M., Ghiorso, M., Davis, F., Gordon, S., Mukherjee, S., Grove, T., Krawczynski, M., Medard, E., and Till, C. (2008) Library of Experimental Phase Relations (LEPR): A database and Web portal for experimental magmatic phase equilibria data. *Geochemistry, Geophysics, Geosystems*, 9.
- Ionov, D., and Wood, B. (1992) The oxidation state of subcontinental mantle: oxygen thermobarometry of mantle xenoliths from central Asia. *Contributions to Mineralogy and Petrology*, 111, 179–193.
- Johnson, K., and Dick, H.J. (1992) Open system melting and temporal and spatial variation of peridotite and basalt at the Atlantis II fracture zone. *Journal of Geophysical Research: Solid Earth*, 97, 9219–9241.
- Keefner, J., Mackwell, S., Kohlstedt, D., and Heidelbach, F. (2011) Dependence of dislocation creep of dunite on oxygen fugacity: implications for viscosity variations in Earth's mantle. *Journal of Geophysical Research: Solid Earth*, 116.
- Kress, V., and Carmichael, I. (1988) Stoichiometry of the iron oxidation reaction in silicate melts. *American Mineralogist*, 73, 1267–1274.
- Kress, V.C., and Carmichael, I.S. (1991) The compressibility of silicate liquids containing Fe₂O₃ and the effect of composition, temperature, oxygen fugacity and pressure on their redox states. *Contributions to Mineralogy and Petrology*, 108, 82–92.
- Lambart, S., Laporte, D., and Schiano, P. (2009) An experimental study of focused magma transport and basalt-peridotite interactions beneath mid-ocean ridges: implications for the generation of primitive MORB compositions. *Contributions to Mineralogy and Petrology*, 157, 429–451.
- Llovet, X., Valovirta, E., and Heikinheimo, E. (2000) Monte Carlo simulation of secondary fluorescence in small particles and at phase boundaries. *Microchimica Acta*, 132, 205–212.
- Luhr, J.F., and Aranda-Gómez, J.J. (1997) Mexican peridotite xenoliths and tectonic terranes: correlations among vent location, texture, temperature, pressure, and oxygen fugacity. *Journal of Petrology*, 38, 1075–1112.
- Mallmann, G., and O'Neill, H.St.C. (2009) The crystal/melt partitioning of V during mantle melting as a function of oxygen fugacity compared with some other elements (Al, P, Ca, Sc, Ti, Cr, Fe, Ga, Y, Zr and Nb). *Journal of Petrology*, 50, 1765–1794.
- Mattioli, G.S., and Wood, B.J. (1988) Magnetite activities across the MgAl₂O₄-Fe₂O₄ spinel join, with application to thermobarometric estimates of upper mantle oxygen fugacity. *Contributions to Mineralogy and Petrology*, 98, 148–162.
- Nasir, S. (1996) Oxygen thermobarometry of the Semail harzburgite massif, Oman and United Arab Emirates. *European Journal of Mineralogy*, 153–164.
- O'Neill, H.St.C., and Wall, V. (1987) The olivine-orthopyroxene-spinel oxygen geobarometer, the nickel precipitation curve, and the oxygen fugacity of the Earth's Upper Mantle. *Journal of Petrology*, 28, 1169–1191.
- Parkinson, I.J., and Arculus, R.J. (1999) The redox state of subduction zones: insights from arc-peridotites. *Chemical Geology*, 160, 409–423.
- Parkinson, I.J., and Pearce, J.A. (1998) Peridotites from the Izu-Bonin-Mariana forearc (ODP Leg 125): evidence for mantle melting and melt-mantle interaction in a supra-subduction zone setting. *Journal of Petrology*, 39, 1577–1618.
- Poustovetov, A., and Roeder, P. (2001) Numerical modeling of major element distribution between chromian spinel and basaltic melt, with application to chromian spinel in MORBs. *Contributions to Mineralogy and Petrology*, 142, 58–71.
- Rampone, E., Hofmann, A.W., and Raczek, I. (1998) Isotopic contrasts within the Internal Liguride ophiolite (N. Italy): the lack of a genetic mantle-crust link. *Earth and Planetary Science Letters*, 163, 175–189.
- Rohrbach, A., Ballhaus, C., Ulmer, P., Golla-Schindler, U., and Schönbohm, D. (2011) Experimental evidence for a reduced metal-saturated upper mantle. *Journal of Petrology*, 52, 717–731.
- Sack, R.O., and Ghiorso, M.S. (1991a) An internally consistent model for the thermodynamic properties of Fe-Mg-titanomagnetite-aluminate spinels. *Contributions to Mineralogy and Petrology*, 106, 474–505.
- (1991b) Chromian spinels as petrogenetic indicators; thermodynamics and petrological applications. *American Mineralogist*, 76, 827–847.
- Smith, P.M., and Asimow, P.D. (2005) *Adiabat_lph*: A new public front-end to the MELTS, pMELTS, and pHMELTS models. *Geochemistry, Geophysics, Geosystems*, 6.
- Stagno, V., and Frost, D.J. (2010) Carbon speciation in the asthenosphere: Experimental measurements of the redox conditions at which carbonate-bearing melts coexist with graphite or diamond in peridotite assemblages. *Earth and Planetary Science Letters*, 300, 72–84.
- Stagno, V., Ojwang, D.O., McCammon, C.A., and Frost, D.J. (2013) The oxidation state of the mantle and the extraction of carbon from Earth's interior. *Nature*, 493, 84–88.
- Stormer, J.C. (1983) The effects of recalculation on estimates of temperature and oxygen fugacity from analyses of multicomponent iron-titanium oxides. *American Mineralogist*, 68, 586–594.
- Voigt, M., and von der Handt, A. (2011) Influence of subsolidus processes on the chromium number in spinel in ultramafic rocks. *Contributions to Mineralogy and Petrology*, 162, 675–689.
- Warren, J.M., and Shimizu, N. (2010) Cryptic variations in abyssal peridotite compositions: evidence for shallow-level melt infiltration in the oceanic lithosphere. *Journal of Petrology*, 51, 395–423.
- Wilke, M., Partzsch, G.M., Bernhardt, R., and Lattard, D. (2005) Determination of the iron oxidation state in basaltic glasses using XANES at the K-edge. *Chemical Geology*, 220, 143–161.
- Wood, B.J. (1990) An experimental test of the spinel peridotite oxygen barometer. *Journal of Geophysical Research: Solid Earth*, 95, 15845–15851.
- Wood, B.J., and Virgo, D. (1989) Upper mantle oxidation state: Ferric iron contents of Iherzolite spinels by ⁵⁷Fe Mössbauer spectroscopy and resultant oxygen fugacities. *Geochimica et Cosmochimica Acta*, 53, 1277–1291.
- Woodland, A.B., Kornprobst, J., and Wood, B.J. (1992) Oxygen thermobarometry of orogenic Iherzolite massifs. *Journal of Petrology*, 33, 203–230.
- Xirouchakis, D., Hirschmann, M.M., and Simpson, J.A. (2001) The effect of titanium on the silica content and on mineral-liquid partitioning of mantle-equilibrated melts. *Geochimica et Cosmochimica Acta*, 65, 2201–2217.
- Zhang, H.L., Cottrell, E., Solheid, P.A., Kelley, K.A., and Hirschmann, M.M. (2018) Determination of Fe³⁺/2Fe of XANES basaltic glass standards by Mössbauer spectroscopy and its application to the oxidation state of iron in MORB. *Chemical Geology*, 479, 166–175.

MANUSCRIPT RECEIVED AUGUST 17, 2017

MANUSCRIPT ACCEPTED MARCH 28, 2018

MANUSCRIPT HANDLED BY DANIEL NEUVILLE

Endnote:

¹Deposit item AM-18-76280, Supplemental Figures and Tables. Deposit items are free to all readers and found on the MSA web site, via the specific issue's Table of Contents (go to http://www.minsocam.org/MSA/AmMin/TOC/2018/Jul2018_data/Jul2018_data.html).